

This is an Open Access document downloaded from ORCA, Cardiff University's institutional repository: <https://orca.cardiff.ac.uk/id/eprint/119230/>

This is the author's version of a work that was submitted to / accepted for publication.

Citation for final published version:

Gao, Ruxin, Zhang, Yahui and Kennedy, David 2019. Topology optimization of sound absorbing layer for the mid-frequency vibration of vibro-acoustic systems. *Structural and Multidisciplinary Optimization* 59 (5), pp. 1733-1746. 10.1007/s00158-018-2156-3

Publishers page: <http://dx.doi.org/10.1007/s00158-018-2156-3>

Please note:

Changes made as a result of publishing processes such as copy-editing, formatting and page numbers may not be reflected in this version. For the definitive version of this publication, please refer to the published source. You are advised to consult the publisher's version if you wish to cite this paper.

This version is being made available in accordance with publisher policies. See <http://orca.cf.ac.uk/policies.html> for usage policies. Copyright and moral rights for publications made available in ORCA are retained by the copyright holders.



1 **Topology optimization of sound absorbing layer for the mid-**
2 **frequency vibration of vibro-acoustic systems**

3

4 Ruxin Gao^a, Yahui Zhang^{a*}, David Kennedy^b

5

6 *^a State Key Laboratory of Structural Analysis for Industrial Equipment, Department of*

7 *Engineering Mechanics, International Center for Computational Mechanics, Dalian*

8 *University of Technology, Dalian 116023, PR China;*

9 *^b School of Engineering, Cardiff University, Cardiff CF24 3AA, Wales, UK*

10

11 Corresponding author:

12 Dr. Y. H. Zhang

13 State Key Laboratory of Structural Analysis for Industrial Equipment, Department of

14 Engineering Mechanics, Dalian University of Technology, Dalian 116023, PR China

15 Email: zhangyh@dlut.edu.cn

16 Tel: +86 411 84706337

17 Fax: +86 411 84708393

18

19

1 **Abstract**

2 Due to the significant difference of dynamic properties between the fluid medium
3 and the structure, when a vibro-acoustic system is subjected to a higher frequency
4 excitation, it may typically exhibit mid-frequency behavior which involves different
5 wavelength deformations and is very sensitive to the uncertainties of the system. This
6 paper deals with optimized distribution of a sound absorbing layer for the mid-frequency
7 vibration of vibro-acoustic systems by using hybrid boundary element analysis and
8 statistical energy analysis. Based on the SIMP approach an artificial sound absorbing
9 material model is suggested and the relative densities of the sound absorbing material are
10 taken as design variables. The sound pressure level at a specified point in the acoustic
11 cavity is to be minimized by distributing a given amount of sound absorbing material. An
12 efficient direct differentiation scheme for the response sensitivity analysis is proposed.
13 Then the optimization problem is solved by using the method of moving asymptotes. A
14 numerical example illustrates the validity and effectiveness of the present optimization
15 model. Impact of the excitation frequency on optimized topology is also discussed.

16 **Keywords:** Mid-frequency; Vibro-acoustic system; Sound absorbing layer; Boundary
17 element; Statistical energy analysis; Dynamic topology optimization

1 Introduction

Vibro-acoustic systems are widely used in vehicles such as automobiles, trains, ships and rocket launchers. These vehicles may be subjected to complex environmental excitations during their operation, resulting in strong structural vibration and harmful high noise levels. Early studies on vibration and noise control (see e.g. Christensen et al. 1998a, b) mainly alter the shape and size of system components to control the generation of noise at the sound source. With the development of topology optimization techniques (Sigmund 2001; Bendsøe and Sigmund 2003), more and more researchers began to study the noise control problem of vibro-acoustic systems by using topology optimization techniques. Yoon et al. (2007) dealt with the problem of topology optimization of vibro-acoustic systems using a mixed finite element (FE) formulation (Zienkiewicz and Taylor 2000; Bathe 2008), in which the acoustic cavity is enclosed by a finite boundary. Kook et al. (2012) proposed a design method for acoustical topology optimization considering human hearing characteristics. Shu et al. (2014) studied the topology optimization of vibro-acoustic systems for minimizing sound pressure by using the level set method. To date, the studies on topology optimization of vibro-acoustic systems have been mainly focused on the optimized distribution of structural materials, while the topology optimization of damping or sound absorbing layers has been rarely involved.

However, the design of a large vehicle should not only consider vibration and noise reduction, but also meet other design requirements including stiffness, strength, stability,

1 aerodynamics and hydrodynamics. Therefore, design methods for vibration and noise
2 reduction by finding the optimized layout of structural material have some limitations. At
3 present, a commonly used method is to place damping material on the surface of a
4 structure and sound absorbing material on the sound propagation path to reduce the
5 acoustic radiation and the reflection or transmission of sound waves, respectively.
6 However, a large area of damping or sound absorbing material will cause a sharp increase
7 in system weight, which will not only affect the system performance but also increase the
8 manufacturing cost. In view of the above situation, topology optimization techniques are
9 used to obtain the optimized layout of damping or sound absorbing layers in a vibro-
10 acoustic system. Dühning et al. (2008) studied the optimized placement of damping panels
11 on walls of acoustic cavities by using the solid isotropic material with penalization (SIMP)
12 method (Sigmund 2001; Bendsøe and Sigmund 2003). The sound level can be
13 significantly reduced by optimizing the distribution of the sound absorbing and reflecting
14 material. Akl et al. (2009) developed a mathematical model to simulate fluid-structure
15 interactions based on FE method. A good agreement was obtained between the results
16 obtained from the mathematical model and those from the experiment. Zhang and Kang
17 (2013) presented a topology optimization model to obtain the optimized layout of a
18 damping layer for minimizing the acoustic radiation of damped thin-walled structures. In
19 their paper, the dynamic coupling between the acoustic medium and the structure is
20 neglected. Then considering the velocity response of the structure which is calculated by

1 FE method as an acoustic excitation, the sound pressure at a reference point is obtained
2 by using the boundary element (BE) method (Ciskowski and Brebbia 1991; Wu 2000).
3 They also proposed a sensitivity analysis scheme using the adjoint variable method. Zhao
4 et al. (2017) studied the optimized design of sound absorbing material distribution within
5 sound barrier structures based on the BE method and the optimality criteria method. A
6 smoothed Heaviside-like function was developed to help the SIMP method to obtain a
7 clear 0-1 distribution. The optimized distribution of the sound absorbing material is
8 strongly frequency dependent according to the results obtained by authors, and the
9 optimization in a frequency band was suggested. Du and Olhoff (2007, 2010) studied the
10 topology optimization problem of vibrating bi-material elastic structures placed in an
11 acoustic medium for minimizing the acoustic radiation and gave a corresponding
12 sensitivity analysis scheme. Their papers assumed that the vibration frequency of a
13 structure has a sufficiently high value, so that the radiation impedance at the structure
14 boundary is approximately equal to the characteristic impedance of the acoustic medium
15 (Lax and Feshbach 1947; Herrin et al. 2003). Thus the sound pressure in the acoustic field
16 can be easily obtained by using a high frequency boundary integral equation. Considering
17 that resonance and wave-propagation problems are known to be highly sensitive towards
18 parameter variations and the conventional robust topology optimization methods for
19 structural problems are not suitable for the acoustic problem, Christiansen et al. (2015)
20 suggested a new double filter approach and obtained highly robust designs for acoustic

1 problem. Christiansen and Sigmund (2015) provide the experimental validation of an
2 acoustic cavity designed using topology optimization with the goal of minimizing the
3 sound pressure locally for monochromatic excitation.

4 Based on deterministic methods, such as the FE method, several of the papers
5 mentioned above studied the topology optimization of vibro-acoustic systems. As the
6 frequency increases, the deformation wavelength of the system components will decrease
7 significantly. A fine mesh is required to capture the detailed deformation, typically six to
8 eight elements per wavelength (Simmons 1991; Steel and Craik 1994), which leads to a
9 large number of degrees of freedom (DOF). The computational cost of element-based
10 techniques typically increases due to decreasing wavelengths and multiple reanalyses in
11 the optimization process (Cotoni et al. 2007). Moreover, as the frequency increases, the
12 response of a system will be more and more sensitive to the uncertainties which are
13 inevitably generated during the manufacturing process. Systems with the same nominal
14 geometric and material parameters may produce different responses. At this point, it
15 makes no sense to analyze only one system, and an estimate of average behavior of an
16 ensemble of similar systems with the same nominal properties might be preferred
17 (Ladeveze et al. 2012). As a common statistical method, statistical energy analysis (SEA)
18 (Lyon and DeJong 1995), can give an average prediction for the statistical behavior of
19 systems with little computational cost. However, the assumptions introduced in SEA can
20 only be satisfied when the system is subjected to sufficiently high frequencies (Lyon and

1 DeJong 1995; Langley 1989a). In addition, based on SEA the properties of a system may
2 be highly generalized as some parameters are independent of the material topology layout,
3 which makes topology optimization impossible.

4 Due to the significant difference of dynamic properties between the fluid medium
5 and the structure, when a vibro-acoustic system is subjected to a higher frequency
6 excitation, it may typically exhibit mid-frequency behavior in which some subsystems
7 are large compared with a wavelength, while others are small compared with a
8 wavelength (Shorter and Langley 2005b). At present, neither the FE method nor SEA can
9 describe the motion of vibro-acoustic systems well. To address this situation, three types
10 of improved methods have been proposed for the mid-frequency vibration of complex
11 systems. The first type aims to extend the effective frequency range of traditional
12 deterministic methods to the mid-frequency domain (see e.g. Langley 1989b; Van
13 Vinckenroy and De Wilde 1995; Harari and Avraham 1997; Pluymers et al. 2007; Hinke
14 et al. 2009; Ma et al. 2015b). The second type aims to relax the assumptions in SEA to
15 extend its application to the mid-frequency domain (see e.g. Keane and Price 1987;
16 Langley 1992; Maxit and Guyader 2003; Mace 2005). The third type combines the
17 deterministic and statistical methods to develop a hybrid model for the mid-frequency
18 vibration of complex systems (see e.g. Zhao and Vlahopoulos 2000; Shorter and Langley
19 2005a, b; Ji et al. 2006; Vergote et al. 2011; Zhu et al. 2014; Ma et al. 2015a; Gao et al.
20 2018). As the most popular hybrid approach, the hybrid FE-SEA method proposed by

1 Shorter and Langley (2005b) divides a complex system into a number of deterministic
2 and statistical subsystems according to the deformation wavelength. The so-called
3 deterministic subsystem which is subjected to long wavelength deformation can be
4 modeled by using the FE method, while the so-called statistical subsystem which is
5 subjected to short wavelength deformation can be modeled by using SEA. The dynamic
6 coupling between the two types of subsystems is described as the reflection and
7 transmission of the vibration wave. Based on the diffuse field reciprocity principle
8 (Shorter and Langley 2005a), a non-iterative relationship between the deterministic and
9 statistical subsystems can be established. Due to the combination of the FE method and
10 SEA, the hybrid FE-SEA method can give an average prediction for the mid-frequency
11 vibration and deal with actual engineering systems. Considering the BE method to
12 describe the motion of an acoustic cavity, Gao et al. (2018) proposed the hybrid BE-SEA
13 method for the mid-frequency vibration of vibro-acoustic systems. Due to the nature of
14 the BE method, the hybrid BE-SEA method not only satisfies the Sommerfeld radiation
15 condition at infinity for exterior acoustic problem, but is also more efficient in the
16 modeling stage. Since hybrid approaches are more appropriate than the traditional method
17 for the mid-frequency of complex systems, Muthalif and Langley(2012) studied the active
18 control of mid-frequency vibration by using the hybrid FE-SEA method as an analysis
19 tool. The optimized skyhook damping value and its location were calculated by using the
20 MATLAB GADS toolbox with combined pattern search and genetic algorithms. By using

1 the hybrid FE-wave based (WB) method, Goo et al. (2017) proposed an efficient topology
2 optimization method for bounded acoustic problems. Their method employs the FE
3 method and WB method to respectively model the design and non-design domains to
4 increase computational efficiency and can thus be applied to higher frequency
5 applications that conventional method takes considerable computation time to manage.

6 The present work studies optimized distribution of a sound absorbing layer for the
7 mid-frequency vibration of vibro-acoustic systems by using the hybrid BE-SEA method.
8 In the topology optimization model, an artificial sound absorbing material model is
9 established by employing the SIMP approach. The design objective is the sound pressure
10 level at a specified point in the acoustic cavity, and the design variables are the relative
11 densities of the sound absorbing material. The corresponding sensitivity analysis scheme
12 is derived by direct differentiation. The basic principles of the hybrid BE-SEA method
13 are outlined in Section 2. The topology optimization problem formulation and the
14 corresponding sensitivity analysis scheme are developed in Section 3. In Section 4, a
15 numerical example is presented to illustrate the efficiency of the hybrid BE-SEA method
16 and the validity of the proposed topology optimization model. The impact of the
17 excitation frequency on optimized topology is also discussed. Finally, conclusions are
18 given in Section 5.

19

2 Basic principles of hybrid BE-SEA method

The hybrid BE-SEA method was proposed by Gao et al. (2018) for the mid-frequency vibration of vibro-acoustic systems based on the concept of the hybrid FE-SEA method. Due to the use of the BE method, the hybrid BE-SEA method provided an appropriate model with modeling advantages when the deterministic part of the model is a relatively large acoustic domain.

Without loss of generality, this section demonstrates the basic principles of the hybrid BE-SEA method. In a vibro-acoustic system, the fluid is confined in a bounded acoustic domain Ω , as shown in Fig. 1, of which the boundary surface Γ_a contains a velocity surface Γ_v , an impedance (sound absorbing) surface Γ_z and an elastic thin-walled structural surface Γ_s . The velocity and impedance boundary conditions are expressed by a generalized equation which can be written as (Wu 2000)

$$\mathbf{v}_n = \mathbf{C}_\beta \mathbf{C}_\gamma - \mathbf{C}_\beta \mathbf{C}_\alpha \mathbf{p} \quad (1)$$

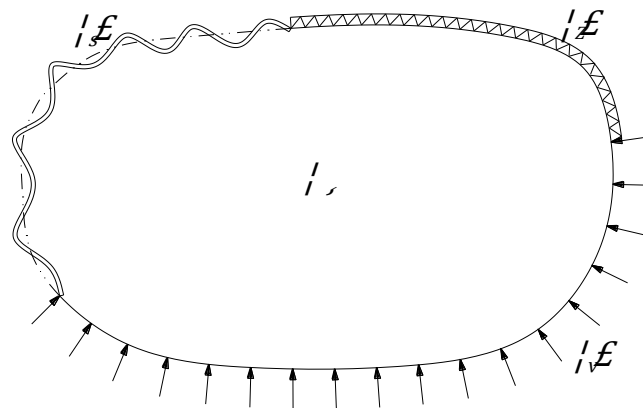


Fig. 1 Coupled vibro-acoustic system. Ω , acoustic domain; Γ_v , velocity boundary surface; Γ_z , impedance boundary surface; Γ_s , elastic thin-structural surface.

1 where the vectors \mathbf{p} and \mathbf{v}_n respectively represent the sound pressures and normal
 2 velocities at nodal points on the boundary of the acoustic cavity. \mathbf{C}_α and \mathbf{C}_β are
 3 constraint coefficient diagonal matrices corresponding to sound pressure and normal
 4 velocity, respectively. \mathbf{C}_γ is a constraint coefficient vector. The hybrid BE-SEA method
 5 (Gao et al. 2018) may be employed for the mid-frequency vibration of the system. The
 6 acoustic cavity modeled by the BE method is treated as the deterministic subsystem, while
 7 the thin-walled structure modeled by SEA is treated as the statistical subsystem.
 8 According to the hybrid BE-SEA method, the response of the statistical thin-walled
 9 structure is viewed as the superposition of the direct and reverberant fields (see Shorter
 10 and Langley 2005a). Considering the velocity and impedance boundary conditions and
 11 the coupling interaction between the acoustic cavity and the direct field of the thin-walled
 12 structure, the governing equation of the system can be written as (Gao et al. 2018)

$$\begin{bmatrix} \tilde{\mathbf{H}} & -i\omega\mathbf{GT} \\ -\mathbf{A} & \mathbf{D}_{\text{dir}} \end{bmatrix} \begin{Bmatrix} \mathbf{p} \\ \mathbf{u} \end{Bmatrix} = \begin{Bmatrix} \mathbf{G}\bar{\mathbf{v}}_n \\ \mathbf{0} \end{Bmatrix} + \begin{Bmatrix} \mathbf{0} \\ \mathbf{f}_{\text{rev}}^s \end{Bmatrix} \quad (2)$$

14
 15 where $\bar{\mathbf{v}}_n = \mathbf{C}_\beta\mathbf{C}_\gamma$, $\tilde{\mathbf{H}} = \mathbf{H} + \mathbf{GC}_\beta\mathbf{C}_\alpha$, \mathbf{H} and \mathbf{G} are the influence matrices of sound
 16 pressure and normal velocity, respectively. \mathbf{D}_{dir} and \mathbf{u} are the dynamic stiffness matrix
 17 and displacement vector of the direct field of the thin-walled structure, respectively. $\mathbf{f}_{\text{rev}}^s$
 18 is the vector of the blocked reverberant forces. \mathbf{A} is a coupling coefficient matrix which
 19 converts the sound pressure vector of the acoustic cavity into the nodal force vector of
 20 the direct field of the thin-walled structure. \mathbf{T} is the transformation matrix resulting from

1 the non-conforming grids appearing at the fluid-structure coupling face, ω is the angular
 2 frequency, and $i = \sqrt{-1}$. For the sake of simplicity, Equation (2) will be written as

$$3 \quad \mathbf{D}_{\text{tot}} \mathbf{q} = \mathbf{f}_{\text{ext}} + \mathbf{f}_{\text{rev}} \quad (3)$$

4 where $\mathbf{D}_{\text{tot}} = \begin{bmatrix} \tilde{\mathbf{H}} & -i\omega \mathbf{G}\mathbf{T} \\ -\mathbf{A} & \mathbf{D}_{\text{dir}} \end{bmatrix}$ and $\mathbf{q} = \begin{Bmatrix} \mathbf{p} \\ \mathbf{u} \end{Bmatrix}$ respectively represent the total dynamic
 5 stiffness matrix and the vector of all deterministic DOF. $\mathbf{f}_{\text{ext}} = \begin{Bmatrix} \mathbf{G}\bar{\mathbf{v}}_n \\ \mathbf{0} \end{Bmatrix}$ and $\mathbf{f}_{\text{rev}} = \begin{Bmatrix} \mathbf{0} \\ \mathbf{f}_{\text{rev}}^s \end{Bmatrix}$
 6 respectively represent the vectors of all external and blocked reverberant forces.
 7

8 If there is sufficient uncertainty in the statistical subsystem, the statistics of the
 9 blocked reverberant force tend to zero (see Shorter and Langley 2005a). Rewriting
 10 equation (3) in cross-spectral form and averaging over an ensemble of statistical thin-
 11 walled structures gives

$$12 \quad \mathbf{S}_{qq} = \langle \mathbf{q}\mathbf{q}^H \rangle = \begin{bmatrix} \mathbf{S}_{pp} & \mathbf{S}_{pu} \\ \mathbf{S}_{up} & \mathbf{S}_{uu} \end{bmatrix} = \mathbf{S}_{qq}^{\text{ext}} + \mathbf{S}_{qq}^{\text{rev}} \quad (4)$$

13 where \mathbf{S}_{qq} represents the cross-spectrum matrix of the deterministic DOF. $\#^H$ is the
 14 Hermitian transpose of $\#$, and $\langle \# \rangle$ is the ensemble average of $\#$. The subscripts p and
 15 u stand for the DOF of the acoustic cavity and the direct field of the thin-walled structure.
 16

17 Also

$$18 \quad \mathbf{S}_{qq}^{\text{ext}} = \mathbf{D}_{\text{tot}}^{-1} \mathbf{S}_{ff}^{\text{ext}} \mathbf{D}_{\text{tot}}^{-H} = \begin{bmatrix} \mathbf{S}_{pp}^{\text{ext}} & \mathbf{S}_{pu}^{\text{ext}} \\ \mathbf{S}_{up}^{\text{ext}} & \mathbf{S}_{uu}^{\text{ext}} \end{bmatrix} \quad (5)$$

$$19 \quad \mathbf{S}_{qq}^{\text{rev}} = \mathbf{D}_{\text{tot}}^{-1} \mathbf{S}_{ff}^{\text{rev}} \mathbf{D}_{\text{tot}}^{-H} = \begin{bmatrix} \mathbf{S}_{pp}^{\text{rev}} & \mathbf{S}_{pu}^{\text{rev}} \\ \mathbf{S}_{up}^{\text{rev}} & \mathbf{S}_{uu}^{\text{rev}} \end{bmatrix} \quad (6)$$

1 where $\mathbf{S}_{ff}^{\text{ext}} = \langle \mathbf{f}_{\text{ext}} \mathbf{f}_{\text{ext}}^{\text{H}} \rangle$ and $\mathbf{S}_{ff}^{\text{rev}} = \langle \mathbf{f}_{\text{rev}} \mathbf{f}_{\text{rev}}^{\text{H}} \rangle$ respectively represent the cross-
 2 spectrum matrices of the total external and blocked reverberant forces. $\#^{-\text{H}}$ represents
 3 the Hermitian transpose of the inverse matrix. Considering the diffuse field reciprocity
 4 principle (see Shorter and Langley 2005a), equation (6) can be rewritten in terms of the
 5 reverberant field energy E and the modal density n_{m} of the thin-walled structure as

$$6 \quad \mathbf{S}_{qq}^{\text{rev}} = \frac{E}{n_{\text{m}}} \frac{4}{\pi\omega} \mathbf{Y} \quad (7)$$

7
 8 where

$$9 \quad \mathbf{Y} = \mathbf{D}_{\text{tot}}^{-1} \text{Im}\{\tilde{\mathbf{D}}_{\text{dir}}\} \mathbf{D}_{\text{tot}}^{-\text{H}} = \begin{bmatrix} \mathbf{Y}_{pp} & \mathbf{Y}_{pu} \\ \mathbf{Y}_{up} & \mathbf{Y}_{uu} \end{bmatrix} \quad (8)$$

10
 11 with

$$12 \quad \tilde{\mathbf{D}}_{\text{dir}} = \begin{bmatrix} \mathbf{0} & \mathbf{0} \\ \mathbf{0} & \mathbf{D}_{\text{dir}} \end{bmatrix} \quad (9)$$

13
 14 The cross-spectrum matrix of the deterministic DOF \mathbf{S}_{qq} can be obtained by using
 15 equations (4)-(9). The only unknown quantity E , at this time, can be calculated by
 16 employing the power balance equation of the reverberant field of the thin-walled structure,
 17 which is given by (see Gao et al. 2018)

$$18 \quad (h_{\text{out}}^{\text{rev}} + h_{\text{diss}}) \frac{E}{n_{\text{m}}} = P_{\text{in}} \quad (10)$$

19
 20 Here, $h_{\text{out}}^{\text{rev}}$ and h_{diss} respectively represent the total energy leaving the reverberant

1 field of the thin-walled structure into the acoustic cavity and the total energy dissipating
 2 by the damping of the thin-walled structure per unit modal energy density in the
 3 reverberant field of the thin-walled structure. $P_{\text{in}} = P_{\text{in}}^{\text{dir}} + P_{\text{in}}^{\text{ext}}$ is the total power input
 4 to the statistical thin-walled structure, where $P_{\text{in}}^{\text{dir}}$ is the power arising from the force
 5 applied to the acoustic cavity and $P_{\text{in}}^{\text{ext}}$ is the power caused by other sources applied
 6 directly to the statistical thin-walled structure. The above parameters can be expressed as
 7

$$P_{\text{in}}^{\text{dir}} = \frac{\omega}{2} \sum_{ij} \text{Im}\{\mathbf{D}_{\text{dir},ij}\}(\mathbf{S}_{uu}^{\text{ext}})_{ij} \quad (11)$$

8

$$h_{\text{diss}} = \omega n_m \eta \quad (12)$$

9

$$h_{\text{out}}^{\text{rev}} = \frac{2}{\pi} \text{Re} \left\{ -i \sum_{ij} \mathbf{C}_{\text{sa},ij} (\mathbf{Y}_{up})_{ij}^* \right\} \quad (13)$$

10

11 where η is the damping loss factor of the thin-walled structure, \mathbf{C}_{sa} is a coupling
 12 coefficient matrix which connects the shape functions of the grids of the acoustic cavity
 13 and the direct field of the thin-walled structure (see Gao et al. 2018). $\#^*$ stands for the
 14 complex conjugate of $\#$.

15 By substituting equations (11)-(13) into equation (10), the ensemble average energy
 16 of the reverberant field can be obtained. The energy of the direct field of the thin-walled
 17 structure can be neglected (see Shorter and Langley 2005b). Hence, by using equations
 18 (4)-(9), \mathbf{S}_{qq} can be calculated. Selecting some points inside the acoustic cavity and

1 calculating the corresponding coefficient matrices \mathbf{g} of sound pressure and \mathbf{h} of
 2 normal velocity, the cross-spectrum matrix of sound pressure at these points can be
 3 expressed as (see Gao et al. 2018)

$$4 \quad \mathbf{S}_{pp}^{\text{in}} = \omega^2(\mathbf{g}\mathbf{T}\mathbf{S}_{uu}\mathbf{T}^H\mathbf{g}^H) + i\omega(\mathbf{\Delta} - \mathbf{\Delta}^H) + \mathbf{\Xi} - \mathbf{\Pi} - \mathbf{\Pi}^H \quad (14)$$

5
 6 where

$$7 \quad \mathbf{\Delta} = \mathbf{g}\mathbf{Q}\mathbf{g}^H + \tilde{\mathbf{h}}\mathbf{S}_{pu}\mathbf{T}^H\mathbf{g}^H \quad (15)$$

$$8 \quad \mathbf{\Xi} = \mathbf{g}\mathbf{S}_{\bar{v}_n\bar{v}_n}\mathbf{g}^H + \tilde{\mathbf{h}}\mathbf{S}_{pp}\tilde{\mathbf{h}}^H \quad (16)$$

$$9 \quad \mathbf{\Pi} = \mathbf{g}\mathbf{S}_{\bar{v}_np}\tilde{\mathbf{h}}^H \quad (17)$$

10
 11 with

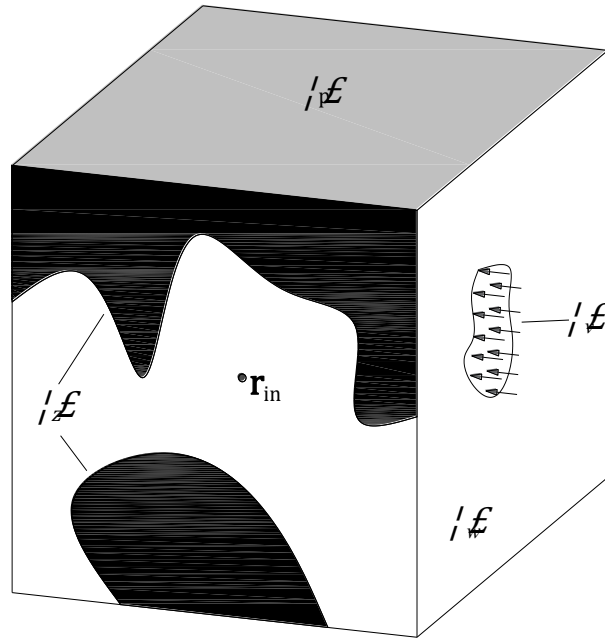
$$12 \quad \mathbf{S}_{\bar{v}_n\bar{v}_n} = \langle \bar{\mathbf{v}}_n\bar{\mathbf{v}}_n^H \rangle \quad (18)$$

$$13 \quad \tilde{\mathbf{h}} = \mathbf{h} + \mathbf{g}\mathbf{C}_\beta\mathbf{C}_\alpha \quad (19)$$

$$14 \quad \mathbf{S}_{\bar{v}_np} = \mathbf{G}^{-1}\tilde{\mathbf{H}}\mathbf{S}_{pp} - i\omega\mathbf{T}\mathbf{S}_{up} \quad (20)$$

$$15 \quad \mathbf{Q} = \mathbf{T}\mathbf{S}_{u\bar{v}_n} = (\mathbf{G}^{-1}\tilde{\mathbf{H}}\mathbf{S}_{\bar{v}_np}^H - \mathbf{S}_{\bar{v}_n\bar{v}_n})/i\omega \quad (21)$$

16
 17 Now inserting equations (15)-(21) into equation (14), $\mathbf{S}_{pp}^{\text{in}}$ can be obtained, and then the
 18 sound pressure level at the points inside the acoustic cavity can be calculated.



1
2 Fig. 2 A vibro-acoustic system with surface sound absorbing layer. Γ_p , a thin plate;
3 Γ_z , the layer of sound absorbing material; Γ_v , the domain subjected to external
4 excitation; Γ_w , the acoustically rigid walls; \mathbf{r}_{in} , a reference point inside the acoustic
5 cavity.

6 **3 Topology optimization problem formulation**

7 **3.1 Topology optimization model**

8 Considering a vibro-acoustic system consisting of a deterministic acoustic cavity
9 and a statistical thin plate as shown in Fig. 2, the acoustic cavity is a cuboid domain
10 coupled with a thin plate on the upper surface. A layer of sound absorbing material is
11 attached to the front surface of the acoustic cavity domain, and a velocity excitation is
12 applied over a region on its right surface. The other regions of the boundary of the acoustic
13 cavity domain are assumed to be acoustically rigid walls. By employing the hybrid BE-
14 SEA method for the mid-frequency vibration of the vibro-acoustic system, this section

1 deals with the optimized layout of a given amount of sound absorbing material within a
 2 prescribed design domain for minimizing the sound pressure level at a specified point
 3 inside the cavity. The topology problem can be thus formulated as

4

$$\left. \begin{aligned}
 &\text{find } \boldsymbol{\rho} = \{\rho_1 \quad \rho_2 \quad \cdots \quad \rho_{m_Z}\}^T \\
 &\text{min } \tilde{S}_{pp}^{\text{in}}(\mathbf{r}_{\text{in}}) = \langle p^* p \rangle \\
 &\text{s. t. } \sum_{k=1}^{m_Z} \rho_k V_k^0 - f_V \sum_{k=1}^{m_Z} V_k^0 \leq 0 \\
 &\quad 0 < \rho_{\min} \leq \rho_k \leq 1 \quad (k = 1, \dots, m_Z)
 \end{aligned} \right\} \quad (22)$$

5

6 where $\boldsymbol{\rho}$ is the vector of the relative density design variables describing layout of the
 7 sound absorbing material. m_Z represents the total number of boundary elements in the
 8 design domain, and each element has one design variable. $\tilde{S}_{pp}^{\text{in}}(\mathbf{r}_{\text{in}})$ represents the
 9 objective function and is a diagonal element of $\mathbf{S}_{pp}^{\text{in}}$ representing the power spectral
 10 density of sound pressure (PSDSP) at a specified point \mathbf{r}_{in} inside the acoustic cavity. It
 11 is important to point out that the objective function can also be written as the sum of the
 12 PSDSPs at more points (i.e. $f = \sum \langle p_i^* p_i \rangle, i = 1, 2 \dots n$) to obtain an overall sound
 13 pressure reduction in the acoustic cavity (Du and Olhoff 2010). f_V represents the volume
 14 fraction and V_k^0 is the volume of sound absorbing material in the k th boundary element
 15 when $\rho_k = 1$. ρ_{\min} is the lower bound of the relative density variables, which is set to
 16 be 10^{-6} to avoid possible numerical singularity.

17 Based on the framework of the SIMP approach, \mathbf{C}_α , \mathbf{C}_β and \mathbf{C}_γ can be
 18 respectively written as

1

$$\mathbf{C}_\alpha = \sum_{k=1}^{m_Z} (\rho_k)^N \mathbf{R}_{\alpha,Z}^{(k)} \quad (23)$$

2

$$\mathbf{C}_\beta = \text{diag}\{\mathbf{E}_v - \mathbf{E}_Z\} \quad (24)$$

3

$$\mathbf{C}_\gamma = \sum_{k=1}^{m_v} \mathbf{v}_0^{(k)} \quad (25)$$

4

5 where $\mathbf{R}_{\alpha,Z}^{(k)}$ is the admittance matrix of the k th element of the sound absorbing layer.

6 The penalty factor $N > 1$ is set to be $N = 3$ in this study. \mathbf{E}_v and \mathbf{E}_Z are location vectors

7 corresponding to velocity and impedance boundary conditions, respectively. $\mathbf{v}_0^{(k)}$ is the

8 velocity vector of the k th element of the velocity surface, and m_v represents the total

9 number of boundary elements on the velocity surface. From equations (24)-(25), it is clear

10 that \mathbf{C}_β and \mathbf{C}_γ remain unchanged during the topology optimization process.

11 3.2 Sensitivity analysis

12 For solving the optimization model of equation (22) with a gradient-based

13 mathematical programming algorithm, it is necessary to perform sensitivity analysis of

14 the objective and constraint functions with respect to the design variables. The sensitivity

15 equation for the PSDSP is derived by direct differentiation, as follows.

16 Differentiating the objective function in equation (22) with respect to the k th design

17 variable gives $\frac{\partial \bar{S}_{pp}^{\text{in}}}{\partial \rho_k}$, a diagonal element of $\frac{\partial \mathbf{S}_{pp}^{\text{in}}}{\partial \rho_k}$ which can be expressed as

18

$$\frac{\partial \mathbf{S}_{pp}^{\text{in}}}{\partial \rho_k} = \omega^2 \left(\mathbf{g} \mathbf{T} \frac{\partial \mathbf{S}_{uu}}{\partial \rho_k} \mathbf{T}^H \mathbf{g}^H \right) + i\omega \left[\frac{\partial \Delta}{\partial \rho_k} - \left(\frac{\partial \Delta}{\partial \rho_k} \right)^H \right] + \frac{\partial \Xi}{\partial \rho_k} - \frac{\partial \Pi}{\partial \rho_k} - \left(\frac{\partial \Pi}{\partial \rho_k} \right)^H \quad (26)$$

1

2 By using equations (15)-(21), $\frac{\partial \Delta}{\partial \rho_k}$, $\frac{\partial \Xi}{\partial \rho_k}$ and $\frac{\partial \Pi}{\partial \rho_k}$ in equation (26) can be, respectively,

3 written as

4

$$\frac{\partial \Delta}{\partial \rho_k} = \mathbf{g} \frac{\partial \mathbf{Q}}{\partial \rho_k} \mathbf{g}^H + \frac{\partial \tilde{\mathbf{h}}}{\partial \rho_k} \mathbf{S}_{pu} \mathbf{T}^H \mathbf{g}^H + \tilde{\mathbf{h}} \frac{\partial \mathbf{S}_{pu}}{\partial \rho_k} \mathbf{T}^H \mathbf{g}^H \quad (27)$$

5

$$\frac{\partial \Xi}{\partial \rho_k} = \frac{\partial \tilde{\mathbf{h}}}{\partial \rho_k} \mathbf{S}_{pp} \tilde{\mathbf{h}}^H + \tilde{\mathbf{h}} \frac{\partial \mathbf{S}_{pp}}{\partial \rho_k} \tilde{\mathbf{h}}^H + \tilde{\mathbf{h}} \mathbf{S}_{pp} \left(\frac{\partial \tilde{\mathbf{h}}}{\partial \rho_k} \right)^H \quad (28)$$

6

$$\frac{\partial \Pi}{\partial \rho_k} = \mathbf{g} \frac{\partial \mathbf{S}_{\bar{v}_n p}}{\partial \rho_k} \tilde{\mathbf{h}}^H + \mathbf{g} \mathbf{S}_{\bar{v}_n p} \left(\frac{\partial \tilde{\mathbf{h}}}{\partial \rho_k} \right)^H \quad (29)$$

7

8 where

9

$$\frac{\partial \tilde{\mathbf{h}}}{\partial \rho_k} = \mathbf{g} \mathbf{C}_\beta \frac{\partial \mathbf{C}_\alpha}{\partial \rho_k} \quad (30)$$

10

$$\frac{\partial \mathbf{S}_{\bar{v}_n p}}{\partial \rho_k} = \mathbf{G}^{-1} \frac{\partial \tilde{\mathbf{H}}}{\partial \rho_k} \mathbf{S}_{pp} + \mathbf{G}^{-1} \tilde{\mathbf{H}} \frac{\partial \mathbf{S}_{pp}}{\partial \rho_k} - i\omega \mathbf{T} \frac{\partial \mathbf{S}_{up}}{\partial \rho_k} \quad (31)$$

11

$$\frac{\partial \mathbf{Q}}{\partial \rho_k} = \mathbf{T} \frac{\partial \mathbf{S}_{u\bar{v}_n}}{\partial \rho_k} = \left(\mathbf{G}^{-1} \frac{\partial \tilde{\mathbf{H}}}{\partial \rho_k} \mathbf{S}_{\bar{v}_n p}^H + \mathbf{G}^{-1} \tilde{\mathbf{H}} \frac{\partial \mathbf{S}_{\bar{v}_n p}^H}{\partial \rho_k} \right) / i\omega \quad (32)$$

12

13 with

14

$$\frac{\partial \tilde{\mathbf{H}}}{\partial \rho_k} = \mathbf{G} \mathbf{C}_\beta \frac{\partial \mathbf{C}_\alpha}{\partial \rho_k} \quad (33)$$

15

16 Substituting equation (27)-(33) into equation (26), it can be seen that $\frac{\partial \mathbf{S}_{pp}^{\text{in}}}{\partial \rho_k}$ is

1 determined by $\frac{\partial \mathbf{C}_\alpha}{\partial \rho_k}$ and $\frac{\partial \mathbf{S}_{qq}}{\partial \rho_k}$. Differentiating equation (23) with respect to the k th design
 2 variable, $\frac{\partial \mathbf{C}_\alpha}{\partial \rho_k}$ can be written as

$$3 \quad \frac{\partial \mathbf{C}_\alpha}{\partial \rho_k} = \sum_{k=1}^m N(\rho_k)^{(N-1)} \mathbf{R}_{\alpha,Z}^{(k)} \quad (34)$$

4
 5 According to equation (4), $\frac{\partial \mathbf{S}_{qq}}{\partial \rho_k}$ can be written as

$$6 \quad \frac{\partial \mathbf{S}_{qq}}{\partial \rho_k} = \frac{\partial \mathbf{S}_{qq}^{\text{ext}}}{\partial \rho_k} + \frac{\partial \mathbf{S}_{qq}^{\text{rev}}}{\partial \rho_k} \quad (35)$$

7
 8 where $\frac{\partial \mathbf{S}_{qq}^{\text{ext}}}{\partial \rho_k}$ and $\frac{\partial \mathbf{S}_{qq}^{\text{rev}}}{\partial \rho_k}$ can be, respectively, obtained by differentiating equations (5) and
 9 (7) with respect to the k th design variable and written as

$$10 \quad \frac{\partial \mathbf{S}_{qq}^{\text{ext}}}{\partial \rho_k} = \boldsymbol{\chi}^{(k)} \mathbf{S}_{qq}^{\text{ext}} + (\boldsymbol{\chi}^{(k)} \mathbf{S}_{qq}^{\text{ext}})^{\text{H}} \quad (36)$$

$$11 \quad \frac{\partial \mathbf{S}_{qq}^{\text{rev}}}{\partial \rho_k} = \frac{4}{\pi \omega n_m} \left(E \frac{\partial \boldsymbol{\Upsilon}}{\partial \rho_k} + \frac{\partial E}{\partial \rho_k} \boldsymbol{\Upsilon} \right) \quad (37)$$

12
 13 with

$$14 \quad \boldsymbol{\chi}^{(k)} = -\mathbf{D}_{\text{tot}}^{-1} \frac{\partial \mathbf{D}_{\text{tot}}}{\partial \rho_k} \quad (38)$$

$$15 \quad \frac{\partial \boldsymbol{\Upsilon}}{\partial \rho_k} = \boldsymbol{\chi}^{(k)} \boldsymbol{\Upsilon} + (\boldsymbol{\chi}^{(k)} \boldsymbol{\Upsilon})^{\text{H}} \quad (39)$$

16
 17 Derivatives of the thin plate energy and the total dynamic stiffness matrix with
 18 respect to the k th design variable respectively appear in equations (37) and (38). By using

19 equations (2), (3) and (33), $\frac{\partial \mathbf{D}_{\text{tot}}}{\partial \rho_k}$ can be expressed as

1

$$\frac{\partial \mathbf{D}_{\text{tot}}}{\partial \rho_k} = \begin{bmatrix} \mathbf{G}\mathbf{C}_\beta \frac{\partial \mathbf{C}_\alpha}{\partial \rho_k} & \mathbf{0} \\ \mathbf{0} & \mathbf{0} \end{bmatrix} \quad (40)$$

2

3 Inserting equations (36)-(40) into equation (35), it can be seen that $\frac{\partial E}{\partial \rho_k}$ is the only4 unknown quantity. Differentiating equation (10) with respect to the k th design variable,

5 yields

6

$$\frac{\partial E}{\partial \rho_k} = \left(\frac{\partial P_{\text{in}}^{\text{dir}}}{\partial \rho_k} n_m - \frac{\partial h_{\text{out}}^{\text{rev}}}{\partial \rho_k} E \right) / (h_{\text{out}}^{\text{rev}} + h_{\text{diss}}) \quad (41)$$

7 By using equations (11) and (13), the partial derivative terms on the right of equation (41)

8 can be written as

9

$$\frac{\partial P_{\text{in}}^{\text{dir}}}{\partial \rho_k} = \frac{\omega}{2} \sum_{ij} \text{Im}\{\mathbf{D}_{\text{dir},ij}\} \left(\frac{\partial \mathbf{S}_{uu}^{\text{ext}}}{\partial \rho_k} \right)_{ij} \quad (42)$$

10

$$\frac{\partial h_{\text{out}}^{\text{rev}}}{\partial \rho_k} = \frac{2}{\pi} \text{Re} \left\{ -i \sum_{ij} \mathbf{C}_{\text{sa},ij} \left(\frac{\partial \mathbf{Y}_{up}}{\partial \rho_k} \right)_{ij}^* \right\} \quad (43)$$

11

12 where $\frac{\partial \mathbf{S}_{uu}^{\text{ext}}}{\partial \rho_k}$ can be obtained from equation (36).

13 The solution procedure for the sensitivity analysis of objective function is

14 summarized below:

15 (i) The plate energy sensitivity with respect to design variables $\frac{\partial E}{\partial \rho_k}$ is obtained by

16 inserting equations (42) and (43) into equation (41);

17 (ii) Substituting equation (41) into equation (37), and using equations (35) and (36), $\frac{\partial \mathbf{S}_{qq}}{\partial \rho_k}$

1 is then calculated;

2 (iii) Inserting equations (27)-(29) into equation (26), and using equations (33)-(35), one
3 can obtain the sensitivity of the cross-spectrum matrix of sound pressure at inner
4 points with respect to design variables $\frac{\partial S_{pp}^{\text{in}}}{\partial \rho_k}$.

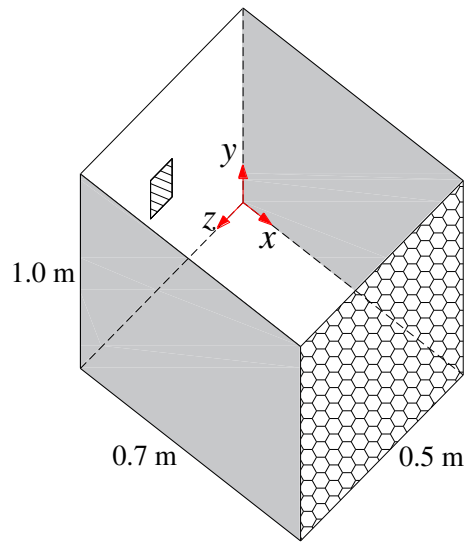
5 (iv) The objective function sensitivity with respect to design variables is calculated by
6 using equation (26).

7 The sensitivity of the constraint function in the optimization model equation (22)
8 with respect to the k th design variable ρ_k equals V_k^0 .

9

10 **4 Numerical example**

11 A simple verification example consisting of two thin plates and an acoustic cavity,
12 as shown in Fig. 3, is presented for illustrating the validity of the proposed topology
13 optimization model. The acoustic cavity is comprised of air and has geometrical
14 dimensions 0.7 m by 1 m by 0.5 m. The sound speed and mass density of the air are
15 $c_0 = 340$ m/s and $\rho_a = 1.225$ kg/m³, respectively. Two thin plates with the same
16 dimensions of 0.7 m by 1.0 m by 1 mm are connected respectively to the front and rear
17 surfaces of the acoustic cavity (the gray areas in Fig. 3). The edges of the two plates are
18 all simply supported, and the in-plane deformation of the two plates is ignored. The two
19 plates are made of aluminum, of which the mass density, Young's modulus, Poisson's
20 ratio and damping loss factor are 2700 kg/m³, 7.1×10^{10} Pa, 0.33 and 0.01, respectively.



1
 2 Fig. 3 Geometric diagram of the vibro-acoustic system. Diagonally hashed area, the
 3 region subjected to velocity excitation; gray area, two plates coupled to the acoustic
 4 cavity; hexagon filled area, the design domain of sound absorbing material layer; other
 5 areas, acoustically rigid walls.

6
 7 The design domain of a sound absorbing layer is connected to the right surface of
 8 the acoustic cavity (the hexagon filled area in Fig. 3). A unit velocity excitation is applied
 9 over a square region (see the diagonal area in Fig. 3) of 0.04 m^2 on the left surface of the
 10 acoustic cavity located at the point $(0, 0.5, 0.25)$. The other areas are considered to be
 11 acoustically rigid.

12 **4.1 Response analysis for the mid-frequency vibration of the vibro-** 13 **acoustic system**

14 In order to show the efficiency of the hybrid BE-SEA method, the responses of the
 15 vibro-acoustic system calculated by employing the hybrid BE-SEA method are compared

1 with those calculated by using Monte Carlo simulation.

2 The impedance of the sound absorbing material is set to be a large real number 10^{40} ,
3 and all element-relative densities of the sound absorbing material in the design domain
4 are set to be 1. The frequency range considered here is from 1 Hz to 400 Hz with a
5 frequency step of 1 Hz. Since the acoustic cavity and each thin plate respectively have 7
6 and 79 modes below 400 Hz, which illustrates the modal density of the acoustic cavity
7 and each plate are significantly different, the systems will exhibit typical mid-frequency
8 vibration behavior consisting of a deterministic acoustical behavior and a statistical
9 structural behavior, within the frequency range of interest. In the hybrid BE-SEA model,
10 the acoustic cavity is modeled by using the BE method, while the two plates are modeled
11 by using SEA. A pure FE model is employed in the Monte Carlo simulation, and a regular
12 fine FE mesh requires to be established to capture detailed deformation. Considering the
13 influence of the uncertainties of the system, an ensemble consisting of 500 samples is
14 generated by randomly choosing 200 points within each plate and adding 0.1% of the
15 mass of one plate at each point.

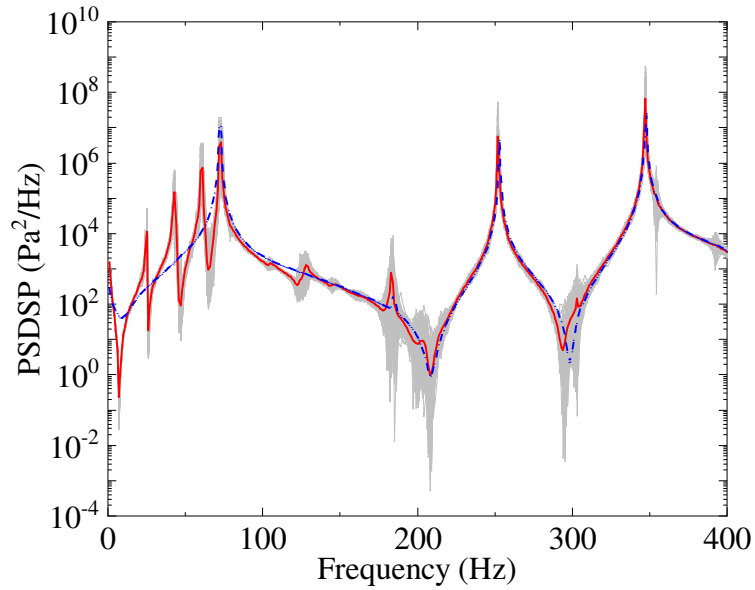
16 It is important to point out that appropriate element sizes should be chosen for the
17 parts modeled using element-based techniques in the two methods, i.e. at least six element
18 per wavelength. Table 1 gives the details of the parts modeled using element-based
19 techniques and the time cost by two methods. As can be seen from Table 1, the minimum
20 number of DOFs and time cost are required for the hybrid FE-SEA method. The hybrid

1 implementations and the Monte Carlo simulation are performed single-threaded in Julia
 2 (v0.6.3.1) on a 3.3 GHz Intel Xeon-based system with a Windows operating system.

3 A comparison of the PSDSP at the point (0.3, 0.6, 0.4) inside the acoustic cavity
 4 calculated by using the hybrid BE-SEA method and the Monte Carlo simulation is shown
 5 in Fig. 4. As can be seen from Fig. 4, the resulting curves of 500 samples are concentrated
 6 at lower frequencies, which confirms that the system uncertainties have little impact on
 7 the system responses when the system is subjected to long wavelength deformation. In
 8 consideration of the sufficient uncertainty the hybrid BE-SEA has assumed over the entire
 9 frequency range, significant discrepancies can be observed between the results calculated
 10 with the two methods at lower frequencies.

11 Table 1 Details of two analysis models

Analysis model		Element type	Element size (m)	Number of elements per wavelength at 400Hz	Number of DOFs	Calculation time (h)
Hybrid BE-SEA	Cavity	4-node quadrilateral	0.050	17	1242	7.9
	Direct field	4-node quadrilateral	0.025	6	1189×2	
Monte Carlo simulation	Cavity	8-node hexahedral	0.025	34	24969	61.4
	Plate	4-node quadrilateral	0.020	6	5508×2	



1

2 Fig. 4 PSDSP at a point inside the acoustic cavity with coordinates (0.3, 0.6, 0.4). Fine

3 solid gray lines, computed using Monte Carlo approach for 500 realizations of

4 ensemble; bold solid red line, ensemble average of Monte Carlo results; bold dash blue

5 line, ensemble average computed using Hybrid BE-SEA method.

6

7 As the frequency increases, the system response becomes very sensitive to the

8 uncertainties of the system, and the resulting curves of 500 samples become dispersed.

9 The hybrid BE-SEA method predicts well the average trend of the pure FE method

10 calculations with perturbed plate mass at higher frequencies. Furthermore, according to

11 the principles of the hybrid BE-SEA method, there is sufficient uncertainty in a statistical

12 subsystem. Hence, it should be pointed out that the average of the Monte Carlo results,

13 which cannot involve all uncertainties (sufficient uncertainty), may have discrepancies

14 with the results obtained by hybrid BE-SEA method even at some higher frequencies

1 (Cotoni et al. 2007; Shorter and Langley 2005b).

2 In this paper, the discrepancies at lower frequencies may be neglected since the
3 attention is only on the mid-frequency vibration of vibro-acoustic systems.

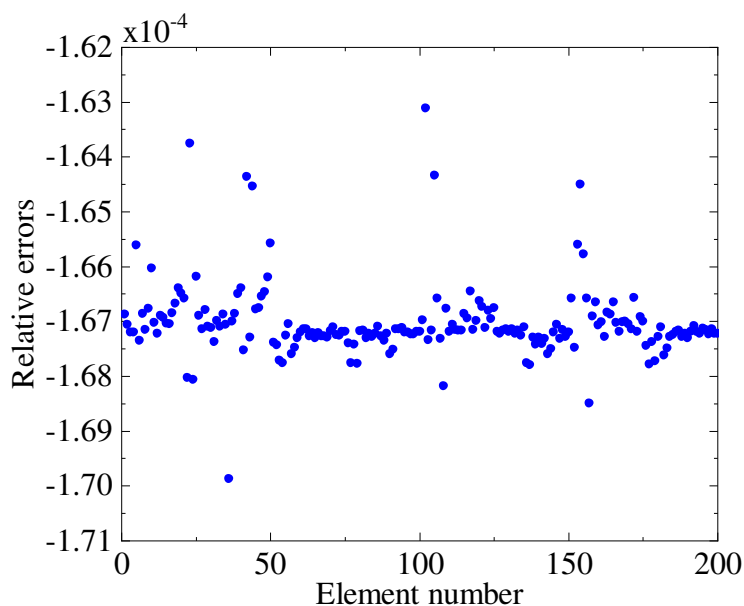
4 5 **4.2 Sensitivity analysis and topology optimization of sound absorbing** 6 **layer for mid-frequency vibration of the vibro-acoustic system**

7 Setting the excitation frequency to be 415 Hz, the partition of the system can be
8 performed by wavelength analysis for the acoustic cavity and the two plates. Here, the
9 acoustic cavity is modeled using the BE method, while the two plates are modeled using
10 SEA. Element sizes chosen for the parts modeled using element-based techniques are the
11 same as those in Table.1. The design domain is discretized by 200 (20×10) uniform-
12 sized square elements. Hence there are 200 design variables $\rho_k (k = 1, 2, \dots, 200)$. The
13 method of moving asymptotes (MMA) (Svanberg 1987, 2002; Johnson 2008, 2014) is
14 employed to update the design variables. The optimization process is stopped when the
15 relative difference of the PSDSP between two adjacent iteration steps is less than 10^{-6} .

16 Sensitivity analysis for the PSDSP is considered first. The point (0.35, 0.50, 0.25) is
17 adopted as the reference point. The impedance of the sound absorbing material is set to
18 be $Z_0 = 975 + 8798i \text{ kg / (m}^2\text{s)}$ (see Siemens Product Lifecycle Management Software
19 Inc 2014), and all element-relative densities of the sound absorbing material in the design
20 domain are set to be 0.6. The relative errors of the sensitivities of the objective function

1 with respect to the design variables $\partial \tilde{S}_{pp}^{\text{in}} / \partial \rho_k (k = 1, 2, \dots, 200)$, calculated by using the
2 present method and the finite difference method (FDM) with 10^{-4} perturbation, are given
3 in Fig. 5.

4 As can be seen from Fig. 5, the comparison shows good agreement. The FDM
5 requires one solution of the linear system of equations for the original value plus one
6 solution (or two if using a central perturbation method) for each design variable. For the
7 present method, one solution of the linear system of equations for the original value is
8 required, and then, according to section 3.2, the derivative (sensitivity) can be calculated
9 directly by a few matrix product operations, without other solutions of the linear system
10 of equations for each design variable. Therefore, compared with FDM, the present method
11 requires less computation time.



12
13 Fig.5 Relative errors of the sensitivities of the PSDSP at the reference point with
14 respect to the element relative density of sound absorbing material.

1 In the following, topology optimization for the vibro-acoustic system is considered.

2 The point (0.60, 0.50, 0.25) is adopted as the reference point. The impedance of the sound

3 absorbing material is set as $Z_0 = 4\rho_a c_0$. All initial design variables are set to be 0.4, and

4 the upper limit of the volume fraction of the sound absorbing material is given as $f_V = 0.5$.

5 The optimization procedure converged after 21 iterations, and the iteration histories of

6 the objective function and volume fraction are shown in Fig. 6. As can be seen, the PSDSP

7 decreases significantly from 196065.61 Pa²/Hz in the initial design to 52063.696 Pa²/Hz

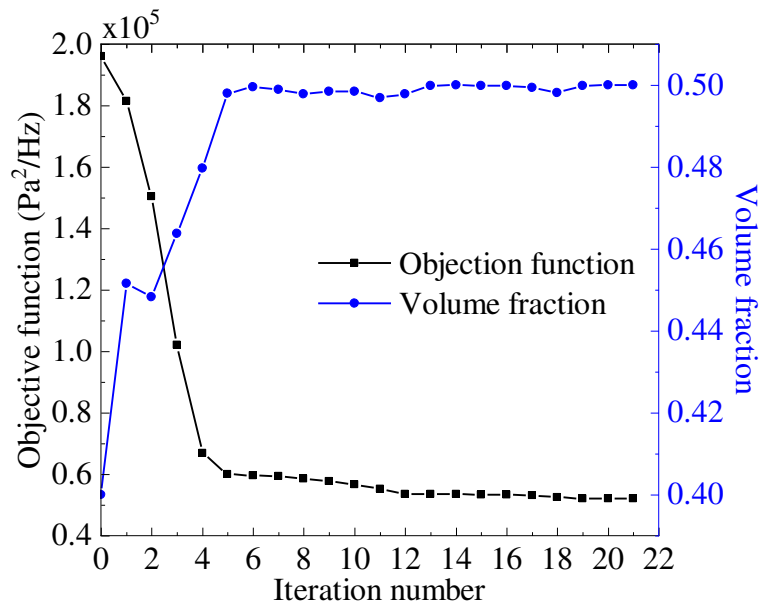
8 in the final optimized design, and the volume fraction of the sound absorbing material

9 reaches the upper limit. The sound absorbing layer layout and the contour of the PSDSP

10 of the design domain for the initial and the optimized design are shown in Fig. 7. As can

11 be seen, the sound absorbing material is concentrated in the places where there is a high

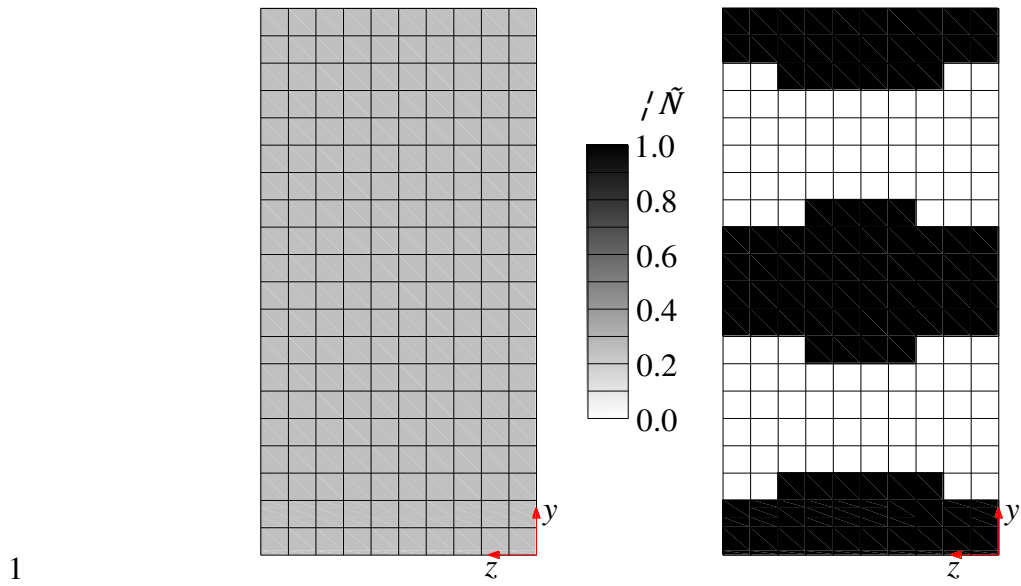
12 PSDSP in the initial design, which indicates that incident sound waves reflect strongly at



13

14

Fig. 6 Iteration histories of objective function and volume fraction.

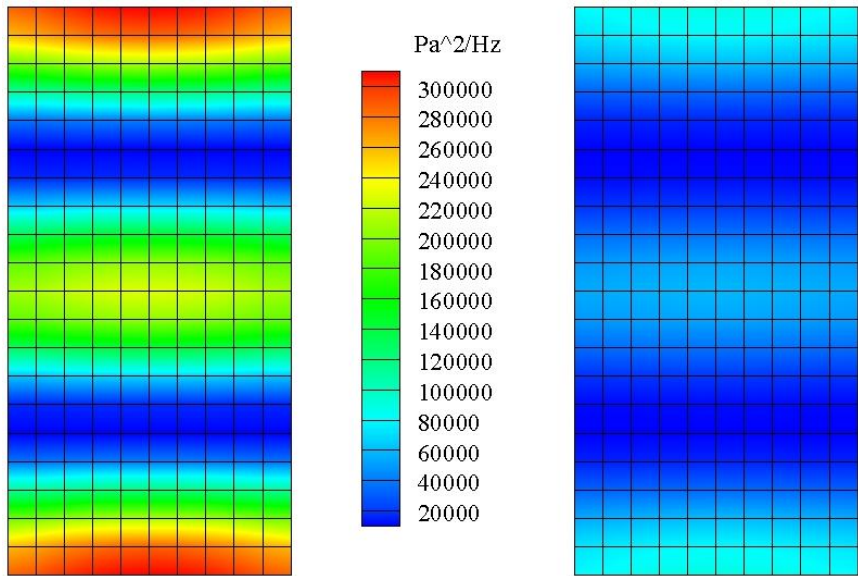


1

(a) Initial design

(b) Optimized design

2



3

(c) Initial design

(d) Optimized design

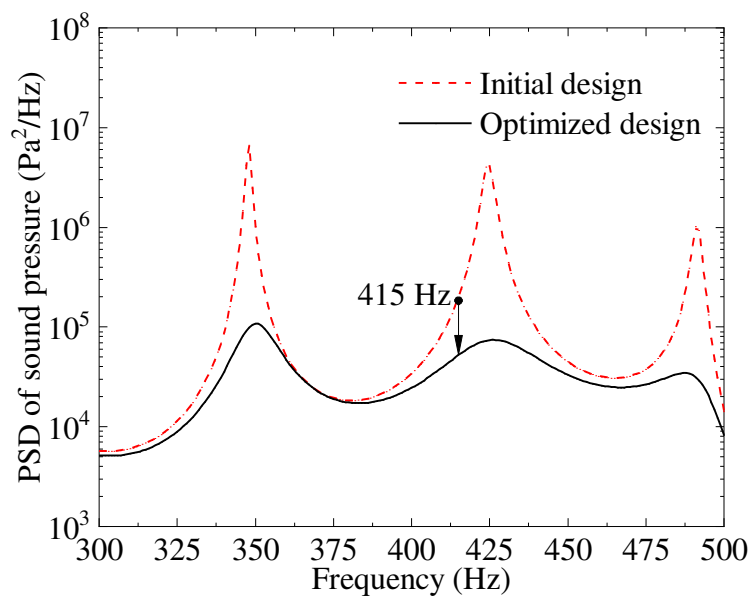
4

5 Fig. 7 Distributions of sound absorbing material for (a) the initial design, (b) the
6 optimized design. The colorbar shows relative density of the sound absorbing material.

7 Contours of the PSDSP for (c) the initial design, (d) the optimized design. The colorbar
8 shows the PSDSP of the design domain.

1 these areas. It can be seen from Fig. 7c and d that the PSDSP of the overall design domain
2 has significantly reduced.

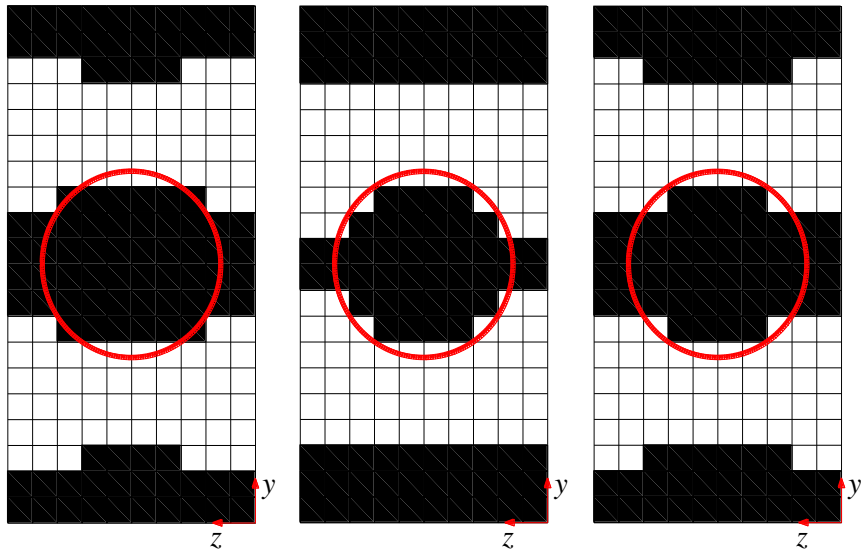
3 Fig. 8 shows curves of PSDSP at the reference point in the frequency range of 300
4 Hz - 500 Hz for the initial and optimized designs. As can be seen, the natural frequencies
5 of the system remain unchanged in the optimization process. Although the excitation
6 frequency selected in the optimization process is 415 Hz, the PSDSP at the reference point
7 decreases over the whole frequency range. However, it is important to point out that the
8 dynamic optimization problem for a vibro-acoustic system is highly nonconvex. A locally
9 optimized design is generally obtained by using a gradient-based mathematical
10 programming algorithm, but such solutions may provide helpful guidance at the
11 conceptual design stage.



12
13 Fig. 8 Curves of PSDSP at the reference point in the frequency range of 300 Hz - 500
14 Hz for the initial and optimized designs.

4.3 Influence of excitation frequencies on optimized designs

In the following, the influence of excitation frequencies on optimized designs is considered. The point (0.60, 0.50, 0.25) is adopted as the reference point. The impedance of the sound absorbing material is set as $Z_0 = 4\rho_a c_0$. All initial design variables are set to be 0.4, and the upper limit of the volume fraction of the sound absorbing material is given as $f_V = 0.5$. The optimization process is performed by selecting the excitation frequencies as 348 Hz, 381 Hz, 425 Hz, 466 Hz, 491 Hz, 300 Hz, 400 Hz and 500 Hz. It can be seen from Fig. 8 that the first five selected frequencies correspond to the three peaks and two valleys of the curve of the PSDSP, and the last three selected frequencies correspond to the beginning, middle and end points of the frequency range of interest.



(a) 348 Hz

(b) 381 Hz

(c) 425 Hz

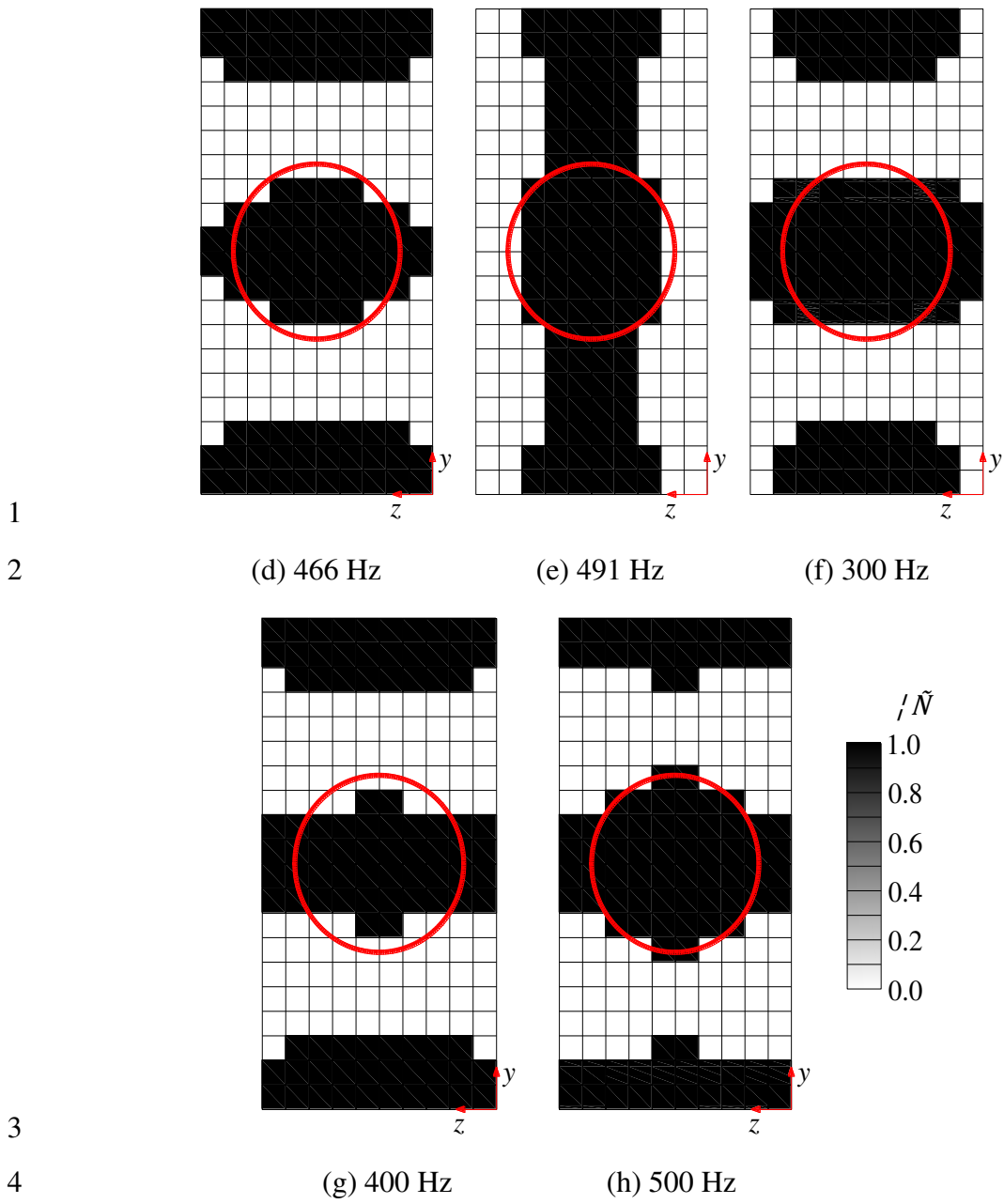


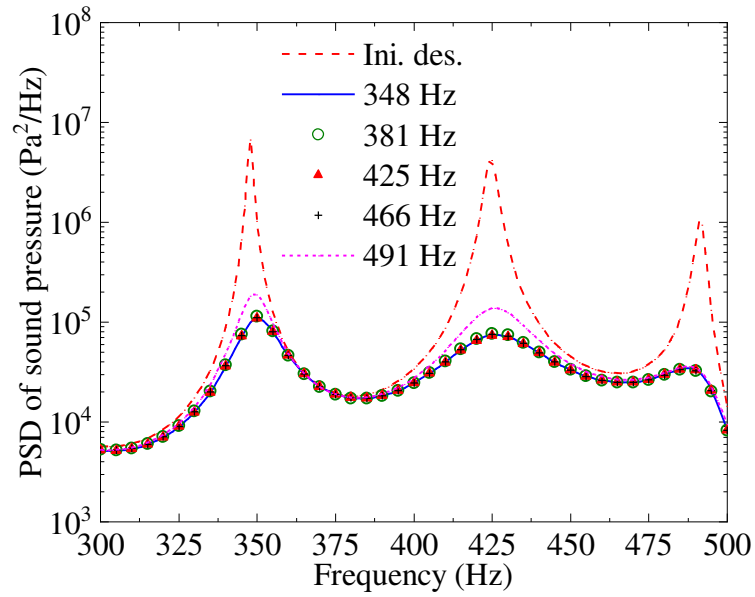
Fig. 9 Optimized design under eight selected excitation frequencies. The colorbar shows relative density of the sound absorbing material.

1 The optimized designs obtained under each excitation frequency are shown in Fig.
2 9. As can be seen, the topology optimization process gives essentially the same optimized
3 designs under most selected excitation frequencies, except for 491 Hz. Moreover,
4 although the optimized design obtained under excitation frequency 491 Hz is obviously
5 different from that obtained under the other seven selected excitation frequencies, the
6 central area of the design domain (the area drawn by the red circle in Fig. 9) is always
7 covered with sound absorbing material, which indicates that incident sound waves reflect
8 strongly at the central area. This is natural since the direction of the velocity excitation
9 points exactly to the central area of the design domain.

10 The first five optimized designs are further studied because the last three optimized
11 designs are very similar to the first three optimized designs. The curves of PSDSP at the
12 reference point in the frequency range of 300 Hz - 500 Hz for the initial and first five
13 optimized designs are shown in Fig. 10. As can be seen, the PSDSP at the reference point
14 decreases over the whole frequency range for the first five optimized designs. In addition,
15 the five curves of PSDSP corresponding to the first five optimized designs are very close,
16 which illustrates the importance of the central area of the design domain.

17 Consider now the topology optimization over the whole frequency band. Selecting
18 3 sampling frequencies (348 Hz, 425 Hz and 491 Hz) in the frequency band of interest,
19 an envelope of the objection function, which is constructed by using a composite
20 Kreisselmeier - Steinhauser objective function (Kreisselmeier and Steinhauser 1979;

1



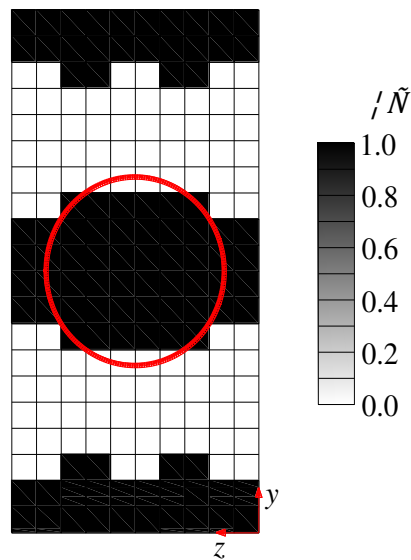
2

3 Fig. 10 Curves of PSDSP at the reference point in the frequency range of 300 Hz - 500

4

Hz for the initial and first five optimized designs.

5



6

7 Fig. 11 Optimized design obtained using an envelope function as the objective

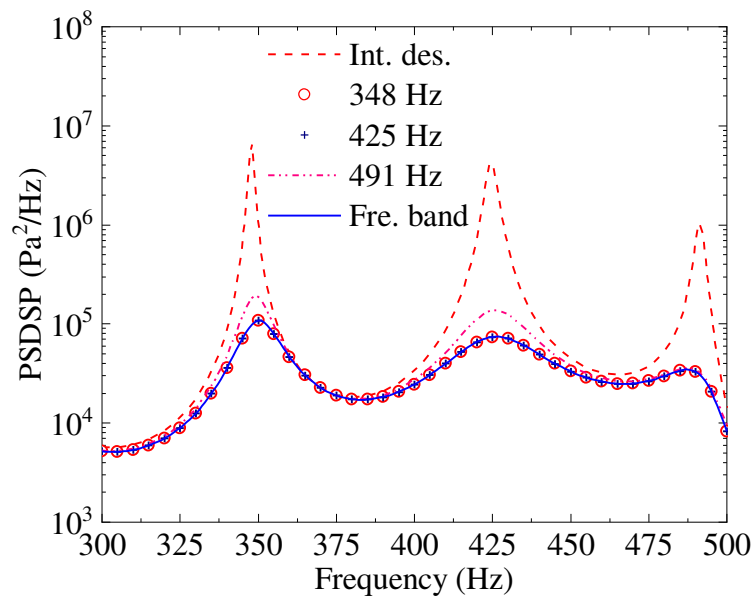
8

function. The colorbar shows relative density of the sound absorbing material.

9

1 Wrenn 1989) with the aggregation parameter $\eta = 1000$, is taken as the objective function
 2 to be minimized.

3 The optimized design obtained using an envelope function over the whole frequency
 4 range as the objective function is shown in Fig. 11. As can be seen, it is almost the same
 5 as the optimized design obtained in Fig. 8 under 348 Hz or 425 Hz. Fig. 12 gives the
 6 comparisons between the PSDSP at the reference point in the frequency range of 300 -
 7 500 Hz for the initial and the optimized designs. As can be seen from Fig. 12, the PSDSP
 8 at the reference point decreases over the whole frequency range for the optimized design
 9 obtained using an envelope function as the objective function. And the optimized design
 10 obtained using an envelope function, not surprisingly, gives almost the same PSDSP at
 11 the reference point as the optimized design obtained under 348 Hz or 425 Hz.



12
 13 Fig. 12 Curves of PSDSP at the reference point in the frequency range of 300 - 500 Hz
 14 for the initial and optimized designs.

1 **5 Conclusions**

2 This paper performs the sensitivity analysis and topology optimization of a sound
3 absorbing layer for minimizing the PSDSP at a specified point in the acoustic cavity when
4 a vibro-acoustic system exhibits mid-frequency behavior. In the topology optimization
5 model, an artificial sound absorbing material model is employed using the SIMP approach
6 and the relative densities of the sound absorbing material are taken as design variables.
7 The PSDSP of the acoustic cavity are calculated by using a hybrid BE-SEA method. In
8 this context, the sensitivity analysis scheme of the PSDSP at a given reference point is
9 developed by using the direct differentiation method. The optimized designs obtained
10 under different excitation frequencies and using an envelope function as the objective
11 function are also compared. The optimization process gives essentially the same
12 optimized designs over a relatively wide frequency range. Moreover, due to the strong
13 reflection of sound waves, the central area in the design domain which faces the region at
14 which the velocity is applied is always covered with sound absorbing material.

15

16 **Acknowledgments**

17 The authors are grateful for support under grants from the National Science
18 Foundation of China (11672060), and the Cardiff University Advanced Chinese
19 Engineering Centre.

1 **References**

- 2 Akl W, El-Sabbagh A, Al-Mitani K, Baz A (2009) Topology optimization of a plate
3 coupled with acoustic cavity. *International Journal of Solids and Structures* 46:2060-
4 2074
- 5 Allaire G, Jouve F, Toader AM (2004) Structural optimization using sensitivity analysis
6 and a level-set method. *Journal of Computational Physics* 194(1): 363-393
- 7 Bathe KJ (2008) *Finite Element Method*. John Wiley & Sons, Inc., Hoboken
- 8 Bendsøe MP (1989) Optimal shape design as a material distribution problem. *Structural*
9 *Optimization* 1(4): 193-202
- 10 Bendsøe MP, Kikuchi N (1988) Generating optimal topologies in structural design using
11 a homogenization method. *Computer Methods in Applied Mechanics and*
12 *Engineering* 71(2): 197-224
- 13 Bendsøe MP, Sigmund O (2003) *Topology Optimization, Theory, Methods and*
14 *Applications*. Springer, Berlin
- 15 Christensen ST, Sorokin SV, Olhoff N (1998a) On analysis and optimization in structural
16 acoustics - Part I: Problem formulation and solution techniques. *Structural*
17 *Optimization* 16(2-3): 83-95
- 18 Christensen ST, Sorokin SV, Olhoff N (1998b) On analysis and optimization in structural
19 acoustics - Part II: Exemplifications for axisymmetric structures. *Structural*
20 *Optimization* 16(2-3): 96-107

- 1 Christiansen RE, Lazarov BS, Jensen JS, Sigmund O (2015) Creating geometrically
2 robust designs for highly sensitive problems using topology optimization. *Structural
3 and Multidisciplinary Optimization* 52: 737-754
- 4 Christiansen RE, Sigmund O (2015) Experimental validation of a topology optimized
5 acoustic cavity. *Journal of the Acoustical Society of America* 138: 3470-3474
- 6 Ciskowski R, Brebbia C (1991) *Boundary Element Methods in Acoustics*. Computational
7 Mechanics Publications, Southampton
- 8 Cotoni V, Shorter P, Langley R (2007) Numerical and experimental validation of a hybrid
9 finite element - statistical energy analysis method. *Journal of the Acoustical Society
10 of America* 122(1): 259-270
- 11 Du J, Olhoff N (2007) Minimization of sound radiation from vibrating bi-material
12 structures using topology optimization. *Structural and Multidisciplinary
13 Optimization* 33(4-5): 305-321
- 14 Du J, Olhoff N (2010) Topological design of vibrating structures with respect to optimum
15 sound pressure characteristics in a surrounding acoustic medium. *Structural and
16 Multidisciplinary Optimization* 42(1): 43-54
- 17 Dühring MB, Jensen JS, Sigmund O (2008) Acoustic design by topology optimization.
18 *Journal of Sound and Vibration* 317(3-5): 557-575
- 19 Gao R, Zhang Y, Kennedy D (2018) A hybrid boundary element-statistical energy
20 analysis for the mid-frequency vibration of vibro-acoustic systems. *Computers and*

- 1 Structures 203: 34-42
- 2 Goo S, Wang S, Kook J, Koo K, Hyun J (2017) Topology optimization of bounded
3 acoustic problems using the hybrid finite element-wave based method. Computer
4 Methods in Applied Mechanics and Engineering 313: 834-856
- 5 Harari I, Avraham D (1997) High-order finite element methods for acoustic problems.
6 Journal of Computational Acoustics 5(1): 33-51
- 7 Herrin DW, Martinus F, Wu TW, Seybert AF (2003) A new look at the high frequency
8 boundary element and Rayleigh integral approximations. Society of Automotive
9 Engineers, Technical Paper 2003-01-1451
- 10 Hinke L, Dohnal F, Mace BR, Waters TP, Ferguson NS (2009) Component mode
11 synthesis as a framework for uncertainty analysis. Journal of Sound and Vibration
12 324(1-2): 161-178
- 13 Ji L, Mace BR, Pinnington RJ (2006) A mode-based approach for the mid-frequency
14 vibration analysis of coupled long- and short-wavelength structures. Journal of
15 Sound and Vibration 289(1-2): 148-170
- 16 Johnson SG (2008) The Nlopt nonlinear-optimization package. [https://nlopt.readthedocs.
17 io/en/latest/](https://nlopt.readthedocs.io/en/latest/)
- 18 Johnson SG (2014) Package to call the NLOpt nonlinear-optimization library from the
19 Julia language. <https://github.com/JuliaOpt/NLOpt.jl>
- 20 Keane AJ, Price WG (1987) Statistical energy analysis of strongly coupled systems.

- 1 Journal of Sound and Vibration 117(2): 363-386
- 2 Kook J, Koo K, Hyun J, Jensen JS, Wang S (2012) Acoustical topology optimization for
3 Zwicker's loudness model - Application to noise barriers. Computer Methods in
4 Applied Mechanics and Engineering 237-240: 130-151
- 5 Kreisselmeier G, Steinhauser R (1979) Systematic control design by optimizing a vector
6 performance index. In: IFAC symposium on computer-aided design of control
7 systems, international federation of active controls. Zurich, Switzerland
- 8 Ladeveze P, Barbarulo A, Riou H, Kovalevsky L (2012) Mid-Frequency - CAE
9 Methodologies for Mid-Frequency Analysis in Vibration and Acoustics. Leuven
10 University Press, Leuven
- 11 Langley RS (1989a) A general derivation of the statistical energy analysis equations for
12 coupled dynamic systems. Journal of Sound and Vibration 135(3): 499-508
- 13 Langley RS (1989b) Application of the dynamic stiffness method to the free and forced
14 vibrations of aircraft panels. Journal of Sound and Vibration 135(2): 319-331
- 15 Langley RS (1992) A wave intensity technique for the analysis of high frequency
16 vibrations. Journal of Sound and Vibration 159(3): 483-502
- 17 Lax M, Feshbach H (1947) On the radiation problem at high frequencies. Journal of the
18 Acoustical Society of America 19(4): 682-690
- 19 Lyon RH, DeJong RG (1995) Theory and Application of Statistical Energy Analysis. 2nd
20 ed., Butterworth-Heinemann, Boston

- 1 Ma Y, Zhang Y, Kennedy D (2015a) A hybrid wave propagation and statistical energy
2 analysis on the mid-frequency vibration of built-up plate systems. *Journal of Sound
3 and Vibration* 352: 63-79
- 4 Ma Y, Zhang Y, Kennedy D (2015b) A symplectic analytical wave based method for the
5 wave propagation and steady state forced vibration of rectangular thin plates. *Journal
6 of Sound and Vibration* 339: 196-214
- 7 Mace BR (2005) Statistical energy analysis: coupling loss factors, indirect coupling and
8 system modes. *Journal of Sound and Vibration* 279(1-2): 141-170
- 9 Maxit L, Guyader JL (2003) Extension of SEA model to subsystems with non-uniform
10 modal energy distribution. *Journal of Sound and Vibration* 265(2): 337-358
- 11 Muthalif AGA, Langley RS (2012) Active control of high-frequency vibration:
12 Optimisation using the hybrid modelling method. *Journal of Sound and Vibration*
13 331(13): 2969-2983
- 14 Pluymers B, Van Hal B, Vandepitte D, Desmet W (2007) Trefftz-based methods for time-
15 harmonic acoustics. *Archives of Computational Methods in Engineering* 14(4): 343-
16 381
- 17 Shorter PJ, Langley RS (2005a) On the reciprocity relationship between direct field
18 radiation and diffuse reverberant loading. *Journal of the Acoustical Society of
19 America* 117(1): 85-95
- 20 Shorter PJ, Langley RS (2005b) Vibro-acoustic analysis of complex systems. *Journal of*

1 Sound and Vibration 288(3): 669-699

2 Shu L, Wang MY, Ma Z (2014) Level set based topology optimization of vibrating
3 structures for coupled acoustic-structural dynamics. Computers and Structures 132:
4 34-42

5 Siemens Product Lifecycle Management Software Inc (2014) LMS Virtual. Lab On-line
6 help. Munich: Siemens AG

7 Sigmund O (2001) A 99 line topology optimization code written in Matlab. Structural and
8 Multidisciplinary Optimization 21(2): 120-127

9 Simmons C (1991) Structure-borne sound transmission through plate junctions and
10 estimates of SEA coupling loss factors using the finite element method. Journal of
11 Sound and Vibration 144(2): 215-227

12 Steel JA, Craik RJM (1994) Statistical energy analysis of structure-borne sound
13 transmission by finite element methods. Journal of Sound and Vibration 178(4): 553-
14 561

15 Svanberg K (1987) The method of moving asymptotes - a new method for structural
16 optimization. International Journal for Numerical Methods in Engineering 24(2):
17 359-373

18 Svanberg K (2002) A class of globally convergent optimization methods based on
19 conservative convex separable approximations. SIAM Journal on Optimization
20 12(2): 555-573

- 1 Van Vinckenroy G, De Wilde WP (1995) The use of Monte Carlo techniques in statistical
2 finite element methods for the determination of the structural behaviour of
3 composite materials structural components. *Composite Structures* 32(1-4): 247-253
- 4 Vergote K, Van Genechten B, Vandepitte D, Desmet W (2011) On the analysis of vibro-
5 acoustic systems in the mid-frequency range using a hybrid deterministic - statistical
6 approach. *Computers and Structures* 89(11-12): 868-877
- 7 Wang MY, Wang X, Guo D (2003) A level set method for structural topology optimization.
8 *Computer Methods in Applied Mechanics and Engineering* 192(1-2): 227-246
- 9 Wrenn G (1989) An indirect method for numerical optimization using the Kreisselmeier
10 - Steinhauser function. Contractor report NASA CR - 4220, NASA Langley
11 Research Center, Hampton, VA, USA
- 12 Wu TW (2000) *Boundary Element Acoustics: Fundamentals and Computer Codes*. WIT,
13 Southampton
- 14 Yoon GH, Jensen JS, Sigmund O (2007) Topology optimization of acoustic-structure
15 interaction problems using a mixed finite element formulation. *International Journal*
16 *for Numerical Methods in Engineering* 70(9): 1049-1075
- 17 Zhang X, Kang Z (2013) Topology optimization of damping layers for minimizing sound
18 radiation of shell structures. *Journal of Sound and Vibration* 332(10): 2500-2519
- 19 Zhao W, Chen L, Zheng C, Liu C, Chen H (2017) Design of absorbing material
20 distribution for sound barrier using topology optimization. *Structural and*

- 1 Multidisciplinary Optimization 56: 315-329
- 2 Zhao X, Vlahopoulos N (2000) Hybrid finite element formulation for mid-frequency
3 analysis of systems with excitation applied on short members. Journal of Sound and
4 Vibration 237(2): 181-202
- 5 Zhou M, Rozvany GIN (1991) The COC algorithm, Part II: Topological, geometry and
6 generalized shape optimization. Computer Methods in Applied Mechanics and
7 Engineering 89(1-3): 309-336
- 8 Zhu D, Chen H, Kong X, Zhang W (2014) A hybrid finite element-energy finite element
9 method for mid-frequency vibrations of built-up structures under multi-distributed
10 loadings. Journal of Sound and Vibration 333(22): 5723-5745
- 11 Zienkiewicz OC, Taylor RL (2000) The Finite Element Method. 5th ed., Butterworth-
12 Heinemann, Oxford
- 13